in silico
Plants
OXFORD

How does structure matter? Comparison of canopy photosynthesis using one- and three-dimensional light models: a case study using greenhouse cucumber canopies

Yi-Chen Pao[1,*], Katrin Kahlen[2], Tsu-Wei Chen[3], Dirk Wiechers[4] and Hartmut Stützel[1]

[1]Institute of Horticultural Production Systems, Leibniz Universität Hannover, 30419 Hannover, Germany
[2]Department of Modeling and Systems Analysis, Hochschule Geisenheim University, 65366 Geisenheim, Germany
[3]Albrecht Daniel Thaer-Institute of Agricultural and Horticultural Sciences, Humboldt-Universität zu Berlin, 10099 Berlin, Germany
[4]KWS SAAT SE & Co. KGaA, 37574 Einbeck, Germany
*Corresponding author's e-mail address: pao@gem.uni-hannover.de

Guest Editor: Kathy Steppe

Editor-in-Chief: Stephen P. Long

Handling Editor: Kathy Steppe

ABSTRACT

One-dimensional light models using the Beer–Lambert equation (BL) with the light extinction coefficient k are simple and robust tools for estimating light interception of homogeneous canopies. Functional–structural plant models (FSPMs) are powerful to capture light–plant interactions in heterogeneous canopies, but they are also more complex due to explicit descriptions of three-dimensional plant architecture and light models. For choosing an appropriate modelling approach, the trade-offs between simplicity and accuracy need to be considered when canopies with spatial heterogeneity are concerned. We compared two light modelling approaches, one following BL and another using ray tracing (RT), based on a framework of a dynamic FSPM of greenhouse cucumber. Resolutions of hourly step (HS) and daily step (DS) were applied to simulate light interception, leaf-level photosynthetic acclimation and plant-level dry matter production over growth periods of 2–5 weeks. Results showed that BL-HS was comparable to RT-HS in predicting shoot dry matter and photosynthetic parameters. The k used in the BL approach was simulated using an empirical relationship between k and leaf area index established with the assistance of RT, which showed variation up to 0.2 in k depending on canopy geometry under the same plant density. When a constant k value was used instead, a difference of 0.2 in k resulted in up to 27 % loss in accuracy for shoot dry matter. These results suggested that, with the assistance of RT in k estimation, the simple approach BL-HS provided efficient estimation for long-term processes.

KEYWORDS: Canopy geometry; dry matter; functional–structural plant model (FSPM); light extinction coefficient; light interception; photosynthetic acclimation.

1. INTRODUCTION

Light is often a limiting factor for greenhouse crops due to 20–70 % reduction by the greenhouse construction (Warren Wilson *et al.* 1992; von Elsner *et al.* 2000; Cabrera-Bosquet *et al.* 2016). As one of the

main greenhouse crops, cucumber plants are mostly trained in high-wire system in a row arrangement (van Henten *et al.* 2002). A row crop system facilitates operations such as plant care and fruit harvest, but results in heterogeneous light distribution in both vertical and

• 1

horizontal directions (Sarlikioti *et al.* 2011b). This condition of limiting and heterogeneous light environment raised the question of suitable methods for modelling light–plant interaction and predicting productivity (Chelle and Andrieu 1999; Roupsard *et al.* 2008; Sarlikioti *et al.* 2011b). Within homogeneous vegetation, intra-canopy light attenuation can be approximated similarly to the light extinction through a turbid medium, by one-dimensional (1D) light models with consideration of limited architectural information such as leaf area index *L*. In this case, vertical light intensity *I* is simulated following Beer–Lambert equation (BL) with a light extinction coefficient *k* (Monsi and Saeki 2005) depicting an exponential decay of incoming light at an incident angle θ with intensity I_0 through canopy depth described by *L*:

$$I = I_0 \times \exp(-k \times L) = I_0 \times \exp\left(\frac{-G_\theta \times \Omega}{\cos\theta} \times L\right) \quad (1a)$$

where G_θ characterizes the leaf projection and accounts for the effects of leaf spatial distribution for intercepting light in the incident direction. In many ecological models a spherical distribution of leaves was assumed, such that G_θ is approximated as 0.5 (Campbell and Norman 1989; Govind 2014). Parameter Ω is the clumping index, and it equals to 1 in the case of random leaf dispersion while it is <1 in the case of clumping (Nilson 1971; Chen and Black 1991), but it is dynamic with θ (Chelle and Andrieu 1999; Govind 2014) and difficult to specify mechanistically (Ponce de León and Bailey 2019). It was found that explicit descriptions of G_θ and Ω are required for adequate approximation of canopy light interception, especially at a $\theta < 70°$ (Govind 2014). The information describing the specific interaction between light and canopy architecture is thus inherently included in *k*. Observed values of *k* were between 0.3 and 2 for different plant functional types (Zhang *et al.* 2014) depending on solar position, leaf angle and clumping (Chen and Black 1991; Monsi and Saeki 2005; Ponce de León and Bailey 2019). Given that canopy light interception depends strongly on characteristics of plant architecture and canopy spacing (Maddonni *et al.* 2001a, b; Sarlikioti *et al.* 2011a; Duursma *et al.* 2012), *k* was also influenced by canopy development (De Costa and Dennett 1992; Chen *et al.* 2014b) and canopy configuration (Nilson 1971; Flénet *et al.* 1996; Drouet and Kiniry 2008; Evers *et al.* 2009; Sarlikioti *et al.* 2011b). Allowing *k* to vary as a function of canopy characteristics was reported to result in better estimations of canopy light interception (Forrester 2014), light transmission (Aubin *et al.* 2000) and transpiration (Tahiri *et al.* 2006). To determine the variation of *k* experimentally, continuous measurements of canopy light transmission and *L*, ideally conducted at a θ near 0° under an overcast sky (Monsi and Saeki 2005), can be rather laborious. A physically based virtual analysis may help better understanding the systematic variation in *k*.

Despite the good approximation of light interception of homogeneous canopies by the 1D approach (Bailey *et al.* 2020), the effects of spatial heterogeneity of local light availability at leaf level cannot be explicitly captured (Chelle and Andrieu 1999; Vos *et al.* 2010). Functional–structural plant models (FSPMs) incorporate three-dimensional (3D) information of plant structure and light models in addition to plant functionality, making it possible to capture feedbacks between canopy architecture and light environment by surface-based models. Such models are especially important for studies considering spatial heterogeneity of environmental factors (Louarn and Song 2020). The heuristic potentials of FSPMs to quantify the effects of canopy architecture on light interception and biomass production have been demonstrated (Sarlikioti *et al.* 2011a; Kang *et al.* 2012; Chen *et al.* 2014b) as well as their capacity to extrapolate and apply knowledge to assist decisions on crop management and breeding (Vos *et al.* 2010; Buck-Sorlin *et al.* 2011; Sarlikioti *et al.* 2011a; Perez *et al.* 2018; Chen *et al.* 2019; N Zhang *et al.* 2020a). Although the capability of handling multiple degrees of complexity is an advantage of FSPMs, it can lead to increased computational requirements and analytical intractability that restrict the range of methods that can be effectively incorporated for model parameterization, analyses, optimization and decision support (Louarn and Song 2020; Zhang and DeAngelis 2020). Despite it not being a major concern nowadays, the complexity of FSPM can still result in various degrees of limitations depending on the hardware and software that are available to the model developers and users. Compared to a simpler model, a more explicit and complex model may better represent the real system up to the point where errors aggravate over the uncertainty of its large amount of parameters (Vos *et al.* 2010).

Therefore, the selection of the degree of simplicity/complexity of an approach to predict spatial heterogeneity and crop productivity should be based on the balance between model accuracy and uncertainty (Renton 2011). In this study, we aimed to examine the trade-offs between simplicity and accuracy of methods simulating light–plant interaction and its influence on long-term leaf-level photosynthetic acclimation and plant-level dry matter accumulation. We compared the two methods, 3D light model using ray tracing (RT) and 1D light model using BL, in a dynamic plant model of greenhouse cucumber. Model performance was evaluated and compared by the predictive accuracy in photosynthetic acclimation and biomass production using both hourly step (HS) and daily step (DS) of time resolutions in order to examine the possible influence of simulation time-step on the predictions.

2. MATERIALS AND METHODS
2.1 Overview of model comparison

A dynamic plant model of greenhouse cucumber was implemented in GroIMP (Kniemeyer 2008) to compare the effect of plant–light interaction methods, recursive RT algorithm and simple BL, on predictive efficiency in photosynthetic acclimation and biomass production. The model described functions of leaf-level photosynthetic acclimation, photosynthesis and plant-level dry matter accumulation, depending on light absorbed by individual leaves as acclimatory signals and driving force (Fig. 1; **see Supporting Information—Fig. S1**). Leaf light interception and absorption was either simulated using BL as 1D light model (red box in Fig. 1), or using RT in a FSPM with 3D descriptions of plant architecture and light model (blue box in Fig. 1; **see Supporting Information—Fig. S1**). Before comparing model predictions of RT and BL, the plant structural traits (lamina area, elevation angle, petiole length and internode length) and light interception efficiency (**Supporting Information—Note S1**, Eq. S1), predicted using RT, were evaluated. Then, RT was used to simulate artificial scenarios of canopy configurations in order to establish a function to estimate light extinction coefficient *k* for use in method BL (Fig. 2). The computer code for the model is available from the corresponding author upon request.
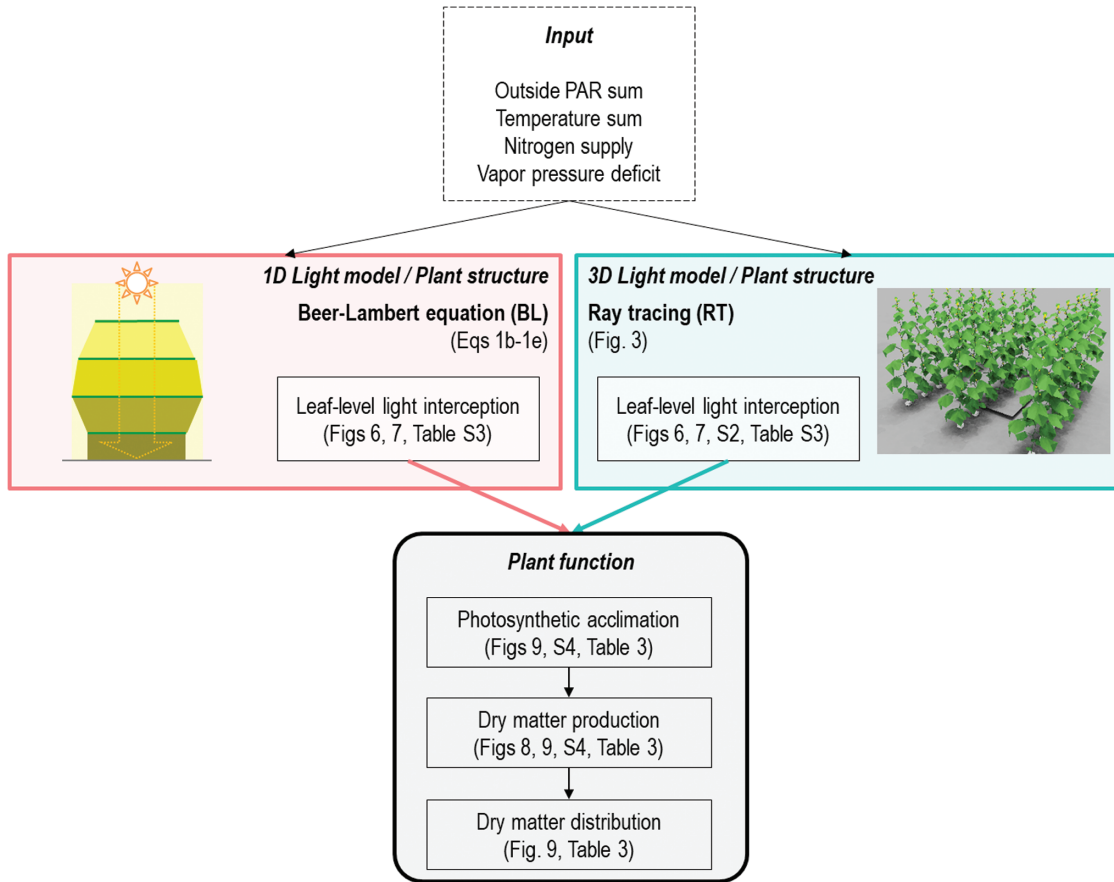
Figure 1. Diagram of model data flow of the dynamic plant model of greenhouse cucumber using light models, the BL (red box) or RT (blue box). Environmental input data (dashed box) given into the model are outside PAR (mol m^{-2} h^{-1}), temperature sum (°Cd), nitrogen supply (mM) and VPD (kPa). Details of *Light model/Plant structure* are shown in **Supporting Information—Fig. S1**. Relevant figures and tables to each variable are indicated in the parentheses.

Model inputs were hourly values of photosynthetically active radiation (PAR$_{out}$, mol m^{-2} h^{-1}) above the greenhouse, temperature sum (°Cd, using 10 °C base temperature for cucumber), nitrogen supply (mM) and relative humidity (%) in the greenhouse. Hourly vapour-pressure deficit (VPD, kPa) was calculated using temperature and relative humidity according to Eq. 12 in Moualeu-Ngangue *et al.* (2016). Simulations were carried out for both HS and DS resolutions. When applying DS, daytime mean VPD (when PAR$_{out}$ > 0.1 mol m^{-2} h^{-1}) and daily temperature sum were calculated from the hourly values. Daily mean photosynthetic photon flux density (PPFD) outside of the greenhouse (I_{out}, μmol m^{-2} s^{-1}) was calculated from PAR$_{out}$ by taking day length (h) into account following a function of Julian day and latitude (°) according to Eqns (1)-(3) in Forsythe *et al.* (1995). Sunrise and sunset were defined as the moment when the top of the sun was apparently even with the horizon.

Intercepted and absorbed PPFD by leaves simulated by both light models were used as input to calculate photosynthetic parameters, photosynthesis and dry matter production (Fig. 1), which were then compared with measured data obtained in greenhouse experiments to evaluate model performance. Root-mean-square deviation (RMSD),

accuracy (%) and relative bias were determined using measured (x_i) and simulated (y_i) values (modified by Kahlen and Stützel 2011):

$$\text{RMSD} = \sqrt{\frac{1}{n}\sum_{i=1}^{n}(y_i - x_i)^2}$$

$$\text{Accuracy}~(\%) = \left(1 - \frac{\text{RMSD}}{\frac{1}{n}\sum_{i=1}^{n}x_i}\right) \times 100$$

$$\text{Relative bias} = \frac{\frac{1}{n}\sum_{i=1}^{n}(y_i)^2 - \frac{1}{n}\sum_{i=1}^{n}(x_i)^2}{\frac{1}{n}\sum_{i=1}^{n}(x_i)^2}$$

2.2 Greenhouse experiments for model evaluation

To obtain measured data of intra-canopy light distribution, architectural traits, leaf photosynthetic parameters and plant dry matter, five experiments (Table 1) were conducted in Venlo-type greenhouses at the Institute of Horticultural Production Systems, Leibniz Universität
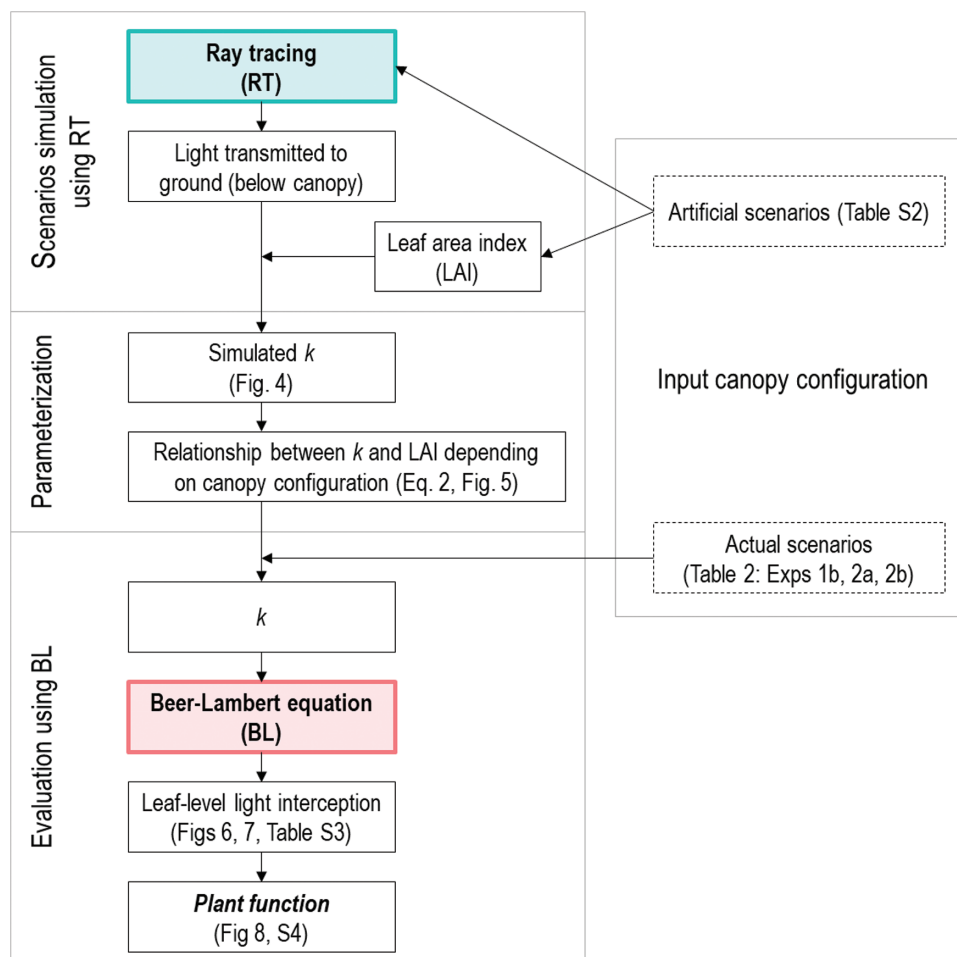
Figure 2. Processes of establishing the relationship between light extinction coefficient k and leaf area index (LAI) using RT, and evaluation of this relationship using the BL. Inputs are indicated in dashed boxes. The relationship between k and LAI was described by Equation (2a) with a minimal k (k_{min}), which was found to be dependent on canopy configuration, and distances between plants and between rows (Equation (2b) and **Fig. 5**). Simulated scenarios of canopy configuration are listed in **Supporting Information—Table S2**, and the simulated k is shown in **Fig. 4**. The canopy configuration of the greenhouse experiments 1b, 2a and 2b (**Table 2**) was used in the evaluation. Relevant figures and tables to each process are indicated in the parentheses.

Table 1. Overview of climate conditions and growth period in the five greenhouse experiments.

Experiment	1a	1b	1c	2a	2b
Time	August 2006	May 2007	August 2007	April 2017	July 2017
Mean temperature (°C)	24.8 ± 2.9	23.2 ± 1.1	23.7 ± 1.6	23.1 ± 0.9	23.9 ± 1.4
Daily PAR integral (mol m^{-2} day^{-1})	24.9 ± 6.7	20.9 ± 7.9	20.5 ± 7.6	22.4 ± 9.6	26.8 ± 10.4
Growth duration in greenhouse (day)	22	30	23	38	38
Julian day	206–227	127–156	211–233	94–131	192–229
Solar zenith angle (°)	32.9–38.5	35.9–30.2	34.0–40.4	46.6–34.7	30.5–39.3

Hannover, Germany (latitude 52.4°N). Experiments 1a, 1b and 1c were conducted in August 2006, May 2007 and August 2007, respectively. Experiments 2a and 2b were conducted in April and July 2017, respectively. In all experiments, cucumber (*Cucumis sativus*) 'Aramon' (Rijk Zwaan, De Lier, The Netherlands) plants were cultivated under a high-wire (up to 4 m) single-stem system in greenhouses oriented from north to south. Three weeks after sowing, five-leaf-stage seedlings in rockwool cubes (10 cm × 10 cm × 6.5 cm) were transferred onto rockwool slabs in the greenhouses and were drip-irrigated with nutrient solution.

Incident PPFD on leaves was measured via PAR sensors on 14 leaves per plant (see Fig. 1a in Wiechers *et al.* 2011b) at the third week after transplanting in experiments 1a, 1b and 1c. In experiments 1b, 2a and 2b, dry matter of leaves, petioles, internodes and fruits per plant was determined destructively with three replications between the second and the fifth weeks after transplanting. Leaf photosynthetic parameters were measured on two leaves per plant with two replications in experiment 2a at the second, third, fourth and fifth weeks after transplanting (Pao *et al.* 2019a). Plant architecture was digitized according to Wiechers *et al.* (2011b) to obtain organ sizes non-destructively in four experiments (1a, 1b, 1c and 2a for lamina size and angle, internode length and petiole length).

In experiments 2a and 2b, plants were grown in rows at a density of 1.33 plants per m² (Table 2). Plants were subjected to treatments of either high light (HL, non-shaded) or low light (LL, reduced by shading to 50 % of HL condition) in combination with either high nitrogen (HN, 10 mM) or low nitrogen (LN, 2.5 mM) supply (for details, see Pao *et al.* 2019a).

In experiments 1a, 1b and 1c, four canopy arrangements (Table 2) of either row (R) or isometric (I) patterns in combination with a density of either 1 (R1 and I1) or 2 (R2 and I2) plants per m² were applied (details see Wiechers *et al.* 2011b), under similar growing conditions as HLHN in experiments 2a and 2b. Plants in experiments 1a and 1c were decapitated above leaf rank 23. The ground in the greenhouses was covered by a white plastic film during experiments 1a–1c.

2.3 Model description—plant development

Virtual plants developed with the appearance of new phytomers. When a meristem reached the thermal age of a phyllochron (°Cd per leaf), the meristem produced a new phytomer. When using the 3D plant architecture model with RT, each phytomer consisted of a meristem, an internode, a petiole and a leaf, represented by 3D objects. When using the 1D model with BL, the organs were not described except that each leaf was assigned the structural property of leaf area index which increased with thermal time. Thermal age of an organ was counted from 0 °Cd starting from the moment of appearance. To mimic the common cultural practice, one flower per node was allowed to develop from the seventh rank of phytomer onwards in the simulation. The ovary reached a length of 5 cm (assumed as starting point of fruit growth) at thermal age of 150 °Cd (ca. 10 days after the appearance of the respective phytomer). Phyllochron needed for a phytomer to appear was described by a logistic function of leaf rank (**Supporting Information—Note S1**, Eq. S2) with an initial phyllochron of 125.4 °Cd at the beginning of plant growth (8–10 days for the first true leaf to appear) and then decreased with increasing rank to stable level of $phyll_{min}$ [see **Supporting Information—Table S1**]. Values of $phyll_{min}$ were derived for each treatment using measured data obtained in experiment 2a, and experiments 1a–1c were assumed to have the same constants as under treatment HLHN.

2.4 Model description—plant function

Photosynthetic acclimation of leaves to light was described by the light response of photosynthetic protein turnover (**Supporting Information—Note S1**, Eqs S3a-e; Pao *et al.* 2019a), the outcome of simultaneous processes of protein synthesis and degradation. Protein synthesis rate was adjusted to an hourly response to PPFD (μmol m^{-2} s^{-1}) by assuming that daily protein synthesis only occurred during the light period. Nitrogen per m² leaf area involved in photosynthetic functions (N_p) of carboxylation (N_V), electron transport (N_J) and light harvesting (N_C) was simulated separately, with initial values of 0.33 mmol m^{-2} each. N_V includes only Rubisco, N_J includes electron transport chain, photosystem II core and Calvin cycle enzymes other than Rubisco and N_C includes photosystem I core and light harvesting complexes I and II (Buckley *et al.* 2013).

Leaf photosynthetic parameters were estimated from N_V, N_J and N_C, namely maximum carboxylation rate (V_{cmax}, μmol CO$_2$ m^{-2} s^{-1}), maximum electron transport (J_{max}, μmol e$^-$ m^{-2} s^{-1}) and leaf chlorophyll (*Chl*, mmol m^{-2}), respectively (see Appendix 'Computing photosynthetic parameters from N pools' by Buckley *et al.* 2013). Electron transport (J, μmol e$^-$ m^{-2} s^{-1}) and carboxylation rate (V_c, μmol CO$_2$ m^{-2} s^{-1}) were calculated depending on incident light according to Eq. 4 and Eq. 5 in Qian *et al.* (2012), respectively. Leaf absorptance (*a*, unitless) was calculated in relation to *Chl* using Eq. 1 in Evans (1993). Newly appeared leaves had a minimum values of $a = 0.13$ due to the initial values of N_C and N_J. Leaf reflectance and transmittance of PAR and red light were assumed $(1 - a)/2$. Respiration rates R_d (μmol CO$_2$ m^{-2} s^{-1}) of leaves were simulated depending on leaf age and incident light following Eq. 10 in Pao *et al.* (2019a). Mesophyll conductance (g_m, mol CO$_2$ m^{-2} s^{-1}) was simulated depending on leaf thermal age and N_p (**Supporting Information—Note S1**, Eq. S4) modified by Pao *et al.* (2019a).

Leaf net photosynthesis rate A_n (μmol CO$_2$ m^{-2} s^{-1}) was determined as the minimum of RuBP carboxylation-limited (A_c, μmol CO$_2$ m^{-2} s^{-1}) and RuBP regeneration-limited (A_j, μmol CO$_2$ m^{-2} s^{-1}) net photosynthesis rate following the biochemical photosynthesis model of Farquhar *et al.* (1980). For details and constants used in this study, please see Eqs 9, 14 and 15 in Pao *et al.* (2019a). To calculate dry matter production, CO$_2$ uptake was converted to plant dry matter by a factor of 0.68 (Warren Wilson *et al.* 1992).

Dry matter distribution between organs was implemented according to Wiechers *et al.* (2011a). In brief, a common pool of was assumed, which was augmented daily by dry matter production plus excess reserves from the previous day. Dry matter was distributed according to a priority scheme for meeting demands of different organs. Meeting maintenance costs (2 % reduction; Marcelis 1994) was the first priority, followed by root, reproductive growth and then vegetative growth.

Dry matter distributed to individual fruits followed the proportion of a fruit's potential growth rate to the total demand of fruits, which was the sum of potential growth rate of all growing fruits in a plant (Wiechers *et al.* 2011a). Fruit abortion and dominance might occur, if the ratio r_{AD} between total supply and total demand of fruits was lower than certain thresholds. When $r_{AD} < 0.3$, fruits with thermal age between 150 and 220 °Cd were aborted (within 5–6 days after fruit length reached 5 cm). When $r_{AD} < 0.8$, dry matter partitioning to individual fruit exhibited dominance favouring earlier initiated fruits. The potential growth rate of a fruit *i* ($R_{PF,i}$, g DM day^{-1}) was estimated equivalent to its potential dry matter, depending on the length of the fruit ($L_{F,i}$, cm) at the previous day (**Supporting Information—Note S1**, Eq. S5). Actual fruit length $L_{F,i}$ was calculated inversely depending on its actual dry matter using **Supporting Information—Note S1**, Eq. S5. The growth duration of a fruit was accumulated from the time when its length had reached 5 cm until harvest (fruit length ≥ 30 cm).

2.5 Model description—plant structure

Lamina expansion and elevation angles were used in both RT and BL methods [**see Supporting Information—Fig. S1**]. Lamina expansion was described for individual leaves depending on their thermal age (°Cd) using a logistic function (see Eq. 5 in Kahlen 2006) with a minimum of 5 cm² and a specific growth rate of 0.0524 °Cd⁻¹. The maximum area of a leaf depended on its acropetal rank following a log-normal curve (see Eq. 1 in Irving and Robinson 2006) with a maximum leaf area A_{Lmax} (cm²) occurring at rank r_{ALmax} and constant k_{AL} determining the shape of the curve [**see Supporting Information—Table S1**]. Lamina elevation angle (range from −90° to 90°) was defined as the angle between the line connecting the base to the tip of the lamina and the horizontal plane. Newly appearing leaves oriented vertically upwards and thus had a maximal elevation angle of 90°, which then decreased with expansion in its lamina size (cm²) followed **Supporting Information—Note S1**, Eq. S6 by a rate constant of 0.0116 cm⁻² to an asymptote of −68.4°. The constants used in lamina expansion and elevation angle were derived from measured data obtained in experiment 2a for each treatment, and experiments 1a–1c were assumed to have the same constants as under treatment HLHN. No leaves were removed in the simulation runs.

Other plant structural characteristics described below were only implemented when RT was used, namely lamina shape, petiole elongation, petiole zenith angle, leaf tropism and fruit radius [**see Supporting Information—Fig. S1**].

Four templates of lamina shape were reconstructed using digitizing data of cucumber leaves (see Fig. 6A in Pao et al. 2020) of various developmental stages (size ranging 0.01–0.11 m²) in experiment 2a to capture the change of shape along leaf expansion. A template was chosen for a given leaf according to its current size, with arbitrary thresholds set at 0.01, 0.05 and 0.07 m². We chose a shape template depending on lamina size due to the topological dependency of growing leaves on their position and size rather than simple isometric scaling (Schmidt and Kahlen 2019). The chosen template was then scaled to the size of the leaf by a factor, calculated as square root of the ratio between leaf size and template leaf size, to adjust the length of the lines constructing the template.

Leaf petiole elongation was described similar to leaf expansion, with a minimum of 1 cm and a specific growth rate of 0.0312 °Cd⁻¹. The maximum length depended on its rank following a log-normal curve with a maximum length L_{Pmax} (cm) occurring at an acropetal rank r_{LPmax}, and a constant k_{LP} determining the shape of the curve [**see Supporting Information—Table S1**]. Petiole zenith angle was only thermal age-dependent, starting with 0° (vertically upwards), and then turning downwards at a rate of 0.3° per °Cd until a maximum of 100° was reached. Leaf petiole radius was set to 0.45 cm.

Phototropism of leaves was simulated as differential growth of the petiole at its base that caused horizontal movement (Kahlen et al. 2008), with initial phyllotaxis set to 137.5°. Virtual leaves were constructed with two halves along the midrib, so that PAR absorbed by the left (PAR_l) and the right (PAR_r) leaf halves could be simulated separately. A leaf moved towards left when PAR_l/PAR_r > 1 until PAR_l/PAR_r = 1, and vice versa. The maximum tropism was assumed to be 30° per day, with a speed of 2° per °Cd, and it stopped when the thermal age of the petiole exceeded 153 °Cd (Kahlen et al. 2008).

Internode elongation was influenced by daily mean temperature and light signals, i.e. incoming PPFD (μmol m⁻² s⁻¹) above the canopy and red/far-red ratio perceived by the internode according to Eqs 1, 3 and 4 in Kahlen and Chen (2015). The red/far-red signal was assumed to be sensed at the time of maximum growth rate (around internode length of 3 cm). Signals of temperature and incoming PPFD sensed were their 4-day mean values, calculated from Day 6 to Day 3 before the internode reached 3 cm. Until reaching 3 cm, internode length was described depending on its thermal age (°Cd) using a logistic function (see Eq. 5 in Kahlen 2006) with a minimum of 1 cm, a specific growth rate of 0.104 °Cd⁻¹ and a maximum of 6 cm. Angles between two adjacent internodes were set randomly to 15–25°. Internode radii were set to 0.48 cm.

Fruit radius ($r_{F,i}$, cm) was calculated depending on current fruit length $L_{F,i}$ (**Supporting Information—Note S1**, Eq. S7, Kahlen and Stützel 2007; Kuwar 2007). Ratio between fruit length and its petiole length was set to 3 with a minimum petiole length of 2 cm. The radius of the fruit petiole was set to 0.25 cm.

2.6 Simulation of light–plant interaction

To test the performance of the simplest form of 1D light model following the BL, the solar angle was not considered in simulations in both HS and DS, meaning that the solar zenith angle θ was assumed to be 0°. To simulate light–plant interaction with the simple BL, PPFD incident perpendicularly on a leaf i (acropetal rank) was calculated as light transmitted through all leaf area index above the leaf (L_{i+1}) by Equation (1a). However, since not all the leaves are horizontally oriented, Equation (1a) had to be adjusted for individual leaves. Three adjustment methods were compared for incident PPFD I_i on leaf rank i, either by the cosine of the lamina elevation angle β_i (°, Pao et al. 2019a) for each leaf i, by k_c (constant within a canopy, Charles-Edwards et al. 1986) or by a rank-specific k_{i+1} for each leaf i:

$$I_i = I_0 \times \exp(-k_c \times L_{i+1}) \times \cos\beta_i \tag{1b}$$

$$I_i = I_0 \times \exp(-k_c \times L_{i+1}) \times k_c \tag{1c}$$

$$I_i = I_0 \times \exp(-k_c \times L_{i+1}) \times k_{i+1} \tag{1d}$$

The value of k_c in both Equations (1b) and (1c) was constant within a given canopy for all ranks of leaves, while k_{i+1} in Equation (1d) depended on L_{i+1}. Theoretically, the value of k can be derived depending on the given solar zenith and leaf angle distribution of the canopy (see Table 1.1 in Campbell and Norman 1989) by assuming distributions of angles normal to the surface of certain geometric forms. Here, we attempted to apply a dynamic 3D model (Fig. 3) to directly quantify *in silico* the values of k of a canopy under the given condition to include the effects of the solar zenith angle and clumping (Equation (1a)). The quantified k was then used to establish an empirical relationship with L at various developmental stages and configurations (Fig. 2 and see below). The cosine correction in Equation (1b) had a significant effect on PPFD incident on the leaf and could lead to a reduction to 0 % or 42.6 % of the PPFD perpendicularly transmitted to the leaf with an elevation angle of 90° (newly appeared leaves) or −64.8° (matured old
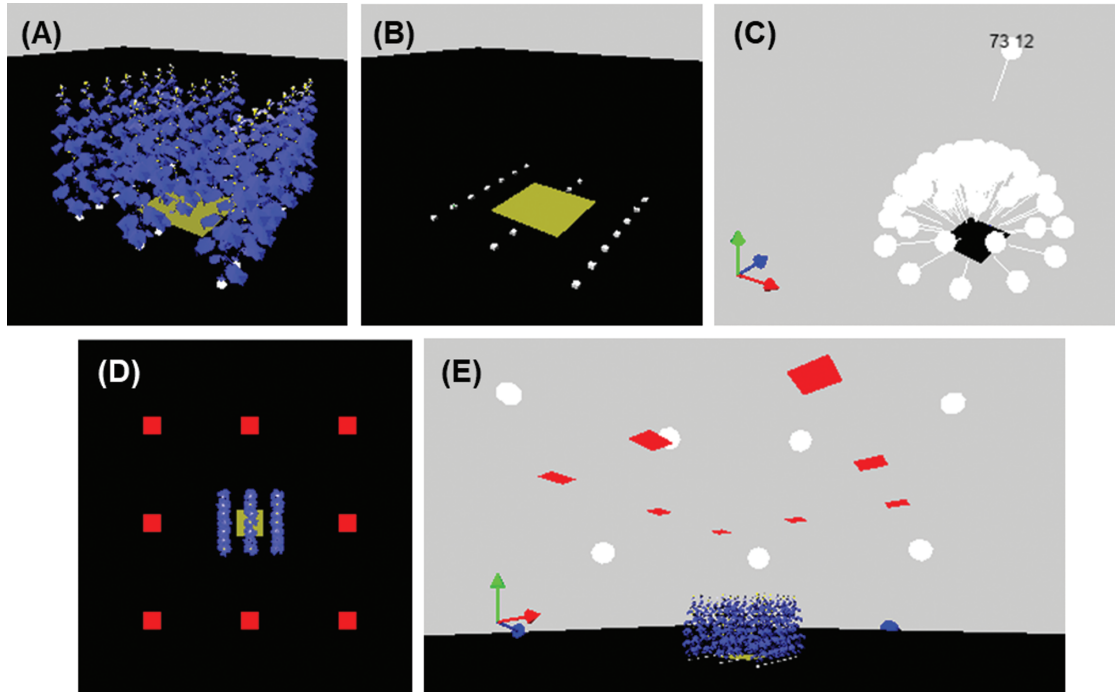
Figure 3. Virtual canopy and light model in the dynamic plant model using RT. (A) A virtual cucumber canopy at a plant density of 1.33 plants per m². The canopies used in the simulations consisted of 21 plants arranged in three north-south oriented rows and seven plants per row. The central three plants in the middle row were sampled for output. (B) Location of rockwool cubes (white squares, height 6.5 cm), from which single virtual plants were grown to form a virtual canopy. A light sensor (yellow square) covering a ground area of three plants was positioned under the canopy 3.5 cm above the rockwool cubes (thus the middle three rockwool cubes are covered). This light sensor had 0 % transmittance and a reflectance similarly to the ground in the corresponding greenhouse experiments. (C) Light model consisting of one direct and 72 diffuse light sources. Blue *y*-axis indicates south in the 3D scene. (D) Positions of eight light sensors (each had a size of 1 m², red squares) for adjusting incident light, viewed from the top and (E) viewed from a side perspective. These eight sensors had 0 % reflectance and 99.9 % transmittance of light and thus negligible interaction with the virtual scene. The yellow and red coloration of the light sensors shown was only for the visualization. The greenhouse structure was not explicitly considered.

leaves), respectively. The *k* correction in Equations (1c) and (1d) on the other hand could restrict PPFD incident on the leaf up to 90 % reduction (if *k* = 0.1) depending on the value of *k*.

To simulate light–plant interactions with the more complex method of the 3D light model, RT, construction of 3D virtual canopies and light sources were required. Virtual canopies were created in the middle on a square ground (60 m × 60 m), which blocked the light cast from below the horizontal plane during simulations in HS. With defined number of rows, number of plants per row and distances between rows and between plants (Table 2), virtual canopies were constructed as mock-up of the actual canopies. In this study, canopies consisting of 21 plants (Fig. 3A) arranged in three north-south oriented rows and seven plants per row were tested. During each simulation, every plant was rotated randomly between −30° to 30° on the horizontal plane to take into account the variation resulting from manual transplanting. The three middle plants in the central row of the canopy were sampled for leaf and plant parameters. A light sensor (blue square in Fig. 3B) was placed 0.1 m above-ground (3.5 cm above the virtual rockwool cubes of the three plants in the middle row, white squares

in Fig. 3B), covering area of a width of one row distance and length of three plant distances in a row. This sensor sampled light transmission to the ground at 1200 h to calculate light extinction coefficients *k* (Equation (1a)) with leaf area index *L* of the canopy. It should be noted that the definition of *L* used here was not the projected leaf area (e.g. Lizaso *et al.* 2005) but the actual leaf area per ground area. In the scenario simulations of *k* under various canopy configurations (Fig. 2), the light sensor below the canopy (Fig. 3B) had light reflectance and transmittance of 0 %, so that it absorbed 100 % of the light incident on it and would not interfere with the 3D scene.

The 3D incoming light was simulated using a light model (Buck-Sorlin *et al.* 2010, 2011) with 72 diffuse light sources (sky objects) arranged in a hemisphere and one directional light source (sun object; Fig. 3C). The light objects cast rays onto the 3D scene, and a ray tracer was integrated to compute light distribution with 10 million rays and a recursion depth of 10 reflections, which was sufficient for simulating PAR at leaf level in rose and cucumber canopies (Buck-Sorlin *et al.* 2011; Chen *et al.* 2014a). The virtual rays consisted of three user-defined channels, which interacted independently with the virtual

Table 2. Canopy configurations of arrangement, plant density and distances between rows and between plants in the five greenhouse experiments.

Experiment	1a/1b/1c				2a/2b
Canopy arrangement	Row (R1)	Row (R2)	Isometric (I1)	Isometric (I2)	Row
Plant density m^{-2}	1	2	1	2	1.33
Row distance (m)	1.86	1.86	0.93	0.93	1.5
Plant distance (m)	0.53	0.27	1.08	0.53	0.5

objects. Due to the light signals concerned in the model, we defined the three channels as PAR, red and far-red light. Optical properties of objects were described according to their absorptance, transmittance and reflectance for each light channel. Optical properties of leaves for PAR and red light depended on *Chl* as described in the plant function section. For simplicity, leaves were assumed to reflect 38 % and transmit 45 % of far-red light (730 nm, Kahlen *et al.* 2008), whereas internodes, petioles and fruits reflect 6 % PAR and red light, and 38 % far-red light with 0 % transmittance of light. A fruit object would no longer interact optically with the virtual scene after it was harvested (0 % reflectance and 100 % transmittance). The ground in the virtual scene did not reflect nor transmit light, thus no reflected light that would affect the light adjustment by the eight light sensors above the ground (Fig. 3D and E). However, the light sensor below the canopy (Fig. 3B) reflected PAR and red light similarly to the ground in the greenhouse experiments 1 and 2, 80 % and 10 %, respectively, during simulations run for evaluation.

The PPFD above the canopy (I_0, μmol m^{-2} s^{-1}) was calculated as 75 % of the PPFD outside the greenhouse (μmol m^{-2} s^{-1}) according to the optical properties of the greenhouse construction. I_0 was then separated according to the proportion of diffuse light (p_{diff}, range 0–1) into light power emitted from the sky objects ($P_{sky} = p_{diff} \times I_0 \times 3 \times f_p$) or from the sun object ($P_{sun} = (1 - p_{diff}) \times I_0 \times 3 \times f_p$). The multiplier 3 accounted for the three light channels. The proportion of diffuse light p_{diff} was calculated following Eq. 3 in Reindl *et al.* (1990), with a clearness index estimated using Eqs 1 and 2 in Hofmann and Seckmeyer (2017). Global radiation R_g (W m^{-2}) was estimated by dividing outside PPFD by 2.07 (PPFD = $R_g \times 0.45 \times 4.6$, assuming 45 % PAR in the global radiation and a conversion factor of 1 W m^{-2} PAR = 4.6 μmol m^{-2} s^{-1}; Ludlow 1983). Since the actual light rays reaching the ground in the 3D scene varied with many factors, such as the angle of the sun object, the proportion of diffuse light and the properties of the ground, a scaling factor f_p was applied to adjust the incoming total light power automatically at every step before simulation according to the amount of light reaching the 3D scene (I_{0sim}). I_{0sim} was measured by eight 1-m^2 sensor objects (around the canopy, Fig. 3D) located at 7 m above the ground (Fig. 3E). These sensor objects were set to have 0 % reflectance and 99.9 % transmittance of light. The maximal value of I_{0sim} from the eight positions was used to compute $f_p = I_0/\max(I_{0sim})$. After the correction using f_p, the deviation of actual PPFD in the 3D scene (at heights up to 5 m above-ground) from I_0 was within 5 %.

Virtual objects absorbed rays that came from all directions into contact according to their optical properties. Light power absorbed by objects was multiplied by 0.33 for red light (assuming one third of

PAR) and by 0.275 for far-red light, shaping a red/far-red ratio of 1.15 in sunlight. Light intensity incident at an object was determined by dividing the absorbed power by the absorptance.

3. RESULTS

3.1 Evaluation of plant structure and light interception predicted by the dynamic plant model using RT

The plant structural traits simulated by the RT model in HS were first compared to digitized data obtained in experiments 1a–1c between ranks 5–20 (total of 191 measured data points from three experiments, four canopy configurations and ca. 16 leaves per plant). The accuracies were 74 %, 73 %, 87 % and 77 % for lamina area, elevation angle, petiole length and internode length, respectively (data not shown). Simulated light interception efficiency (ranging 0–1, **Supporting Information—Note S1**, Eq. S1) showed an accuracy of 73 % with a RMSD of 7.5 % [see **Supporting Information—Fig. S2**], which can be considered a reasonable approximation of the 3D plant structure and light interception.

3.2 Simulations of light extinction coefficient using RT under artificial scenarios

In order to compare predictions of photosynthetic acclimation and dry matter production between RT and by the classic BL, light extinction coefficient *k* had to be first determined for BL (Equations (1b–1d)). Due to the clear effect of canopy configuration on *k* [see **Supporting Information—Fig. S3**], we first simulated *k* under scenarios of different canopy configurations in row arrangements (Fig. 2) using RT throughout the canopy development (growth period of 35 days) every day at midday (1200 h) in DS (Fig. 4). Canopy configurations with various plant densities (1.0, 1.5, 2.0, 2.5 and 3.0 plants per m^2) were created in combination with three different row distances (1.1, 1.5 and 1.9 m), so that plant distance within rows was always smaller than row distance [see **Supporting Information—Table S2**]. These artificial scenarios were selected to cover the common range used in production and experiments. Since there was no apparent difference in simulated *k* between experiments 1a, 1b and 1c within a given canopy configuration [see **Supporting Information—Fig. S3**], only the conditions of experiment 1a were used in this simulation.

Simulated *k* was found to decrease with increasing canopy leaf area index *L*, which could also be interpreted as canopy depth (Fig. 4). This was expectable, since that increasing proportion of expanded leaves approaching an elevation angle of −68.4° (**Supporting Information—Note S1**, Eq. S6) along canopy development allowed

higher light penetration through the canopy and also less efficient light interception towards the base of the canopy. It was observed that denser canopies and wider row distances resulted in lower k (Fig. 4); row distance could lead to a variation in k of up to 0.2 under the same plant density for canopies with $L \geq 1.0$.

3.3 Relationship between light extinction coefficient and leaf area index as depending on canopy geometry

From the results of simulated k under various scenarios of canopy configuration (Fig. 4), an empirical relationship between k and L was derived following a log-normal function, where a maximal k of 1 occurred at L equal to l_m (0.0479 ± 0.0022), with coefficient v_k (1.90 ±
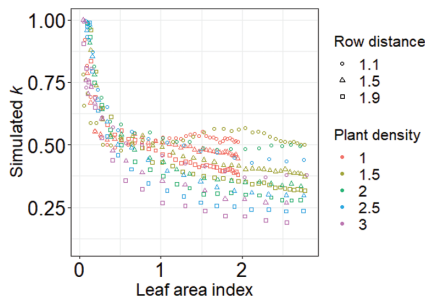

Figure 4. Simulated relationship between light extinction coefficient k and leaf area index of the canopies under scenarios of different plant densities (1.0, 1.5, 2.0, 2.5 and 3.0, indicated by colours; see **Supporting Information—Table S2**) and row distances (1.1, 1.5 and 1.9 m, indicated by symbols). Each point represents one estimate of k for a canopy on a specific day sampled at 1200 h using the FSPM with RT and simulations in HS. Since there was no apparent difference in simulated k between experiments 1a, 1b and 1c [see **Supporting Information—Fig. S3**], only the conditions of experiment 1a with a growth period of 35 days were used in this simulation.
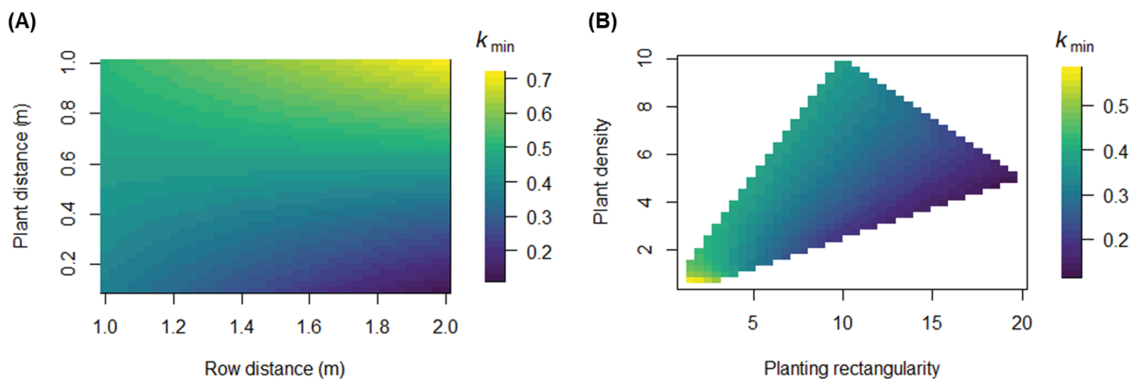
0.056) determining the shape of the curve. Along canopy development, k approached a stable minimal k (k_{min}), which was related to plant distance D_{plant} and row distance D_{row} of the canopy:

$$k = (1 - k_{min}) \times \exp \left\{ - \left[\ln \left(\frac{L}{l_m} \right) / v_k \right]^2 \right\} + k_{min} \tag{2a}$$

$$k_{min} = a_1 - a_2 \times D_{plant} - a_3 \times D_{row} + a_4 \times D_{plant} \times D_{row} \tag{2b}$$

where coefficients were estimated to be a_1 = 0.659 (± 0.0134), a_2 = 0.348 (± 0.0744), a_3 = 0.302 (± 0.0219) and a_4 = 0.502 (± 0.0537). The six parameters in both Equations (2a) and (2b) were quantified with all simulated data of k in Fig. 4 using least square fitting.

Equation (2b) resulted in k_{min} between 0.1 and 0.7 under D_{plant} ranging 0.1–0.9 m and D_{row} ranging 1.0–2.0 m (Fig. 5A). An index of canopy geometry, planting rectangularity (PR; Maddonni *et al.*, 2001b), was calculated using D_{row} and D_{plant} as the ratio between the longer and the shorter distances. In addition to plant density, PR provided information of the geometry of planting patterns. Planting rectangularity equal to 1 indicates a square spatial arrangement, whereas larger values indicate a rectangular geometry. Canopies with more even distribution (PR < 4) appeared to have higher k_{min} under lower plant density (Fig. 5B). However, over a certain level of PR, higher plant density tended to have higher k_{min} (Fig. 5B). With information of canopy configuration in greenhouse experiments 2a and 2b, k_{min} was determined 0.409 with D_{plant} = 0.5 m and D_{row} = 1.5 m. For canopy configurations used in experiment 1b, k_{min} was determined 0.408, 0.255, 0.507 and 0.441 for canopy arrangements R1, R2, I1 and I2, respectively.

3.4 Comparison of leaf-level light availability simulated using RT and using the BL

Equation (2) was applied to simulated k_c and k_{i+1} used in the BL Equations (1b–1d) for further simulations of light interception, photosynthetic acclimation and dry matter production under the conditions of experiment 2a. In Equations (1b–1d), k_c was determined using

Figure 5. Simulated minimal light extinction coefficient k_{min} using Equation (2b) under various canopy configurations. Colour indicates the value of k_{min} (A) at a given distance between rows (1.0–2.0 m) and distance between plants in a row (0.1–1.0 m), (B) under given PR (1.0–20.0, unitless) and plant density (0.5–10.0 plants per m²). Values of k_{min} ranged from 0.12 to 0.71. Planting rectangularity was calculated using row and plant distances as the ratio between the longer and the shorter distances. A PR equal to 1 indicates quadratic canopy geometry, whereas larger values indicate rectangular geometry.

Equation (2a) with L of a canopy at a given time point. In Equation (1d), k_{i+1} was calculated using Equation (2a) for each leaf i with L above it in the canopy (L_{i+1}).

Using the simulation at the end of experiment 2a at 1200 h, a snapshot of intra-canopy relative PPFD was in a comparable range for RT and BL (Fig. 6A) using both HS and DS time resolutions. Relative PPFD at leaf level (I_i/I_0) at a given time point was calculated as the incident PPFD on a leaf at rank i (I_i) divided by the PPFD above the canopy (I_0). Different BL equations resulted in large variation in I/I_0 at
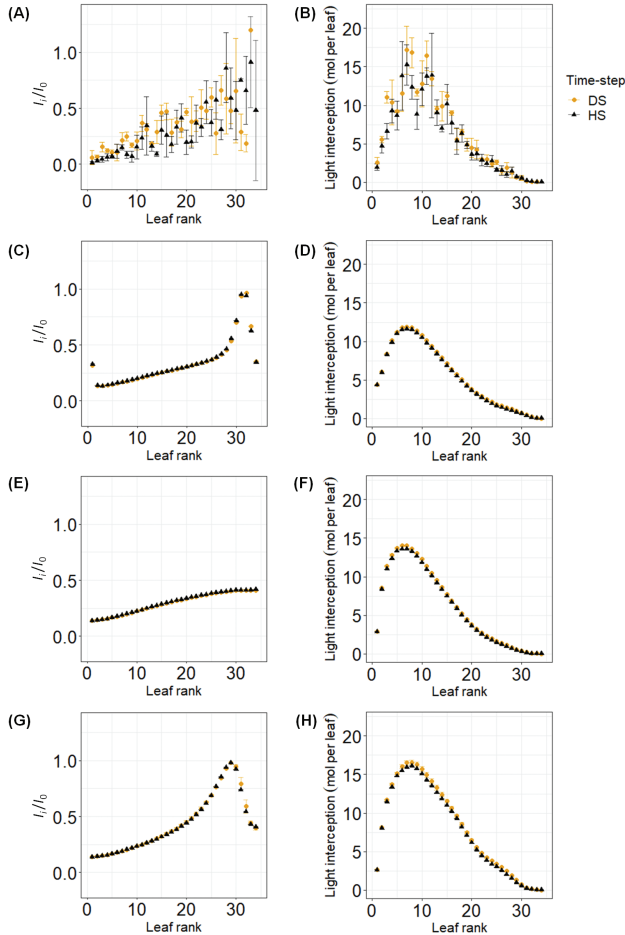

Figure 6. Comparison of simulated light conditions at leaf level using different light models and time resolutions. The models compared were (A, B) RT and (C–H) the BL in DS (yellow circles) or HS (black triangles). Different methods of BL were compared, namely using Equation (1b) (C, D), Equation (1c) (E, F) and Equation (1d) (G, H). (A, C, E, G) Snapshot of simulated relative PPFD (I_i/I_0) at 1200 h on the last day of a 5-week growth period, calculated as incident PPFD at each leaf divided by PPFD level above the canopy. (B, D, F, H) Total light interception (mol per leaf) summed over the 5-week growth period under the conditions of experiment 2a and treatment HLHN (for other treatments, see **Supporting Information—Table S3**).

higher ranks (≥20, young leaves) without systematic deviation from I/I_0 predicted using RT. At the lower ranks, the variation in I/I_0 between BL equations became subtle. The light model BL using Equations (1b) and (1d) seemed to better capture the variability of I_i/I_0 by RT at the higher ranks, which was not observed when applying Equation (1c). However, Equation (1c) rather predicted the middle-lower range of I_i/I_0 variability at the higher ranks.

Total light interception by individual leaves (mol per leaf, Fig. 6B) over 5 weeks of growth period was also simulated under the conditions of experiment 2a. Regardless of the approach used, the middle-lower layer of the canopy contributed largely to total light interception (Fig. 6B). Total light interception simulated using BL (1b) was 77–92 % of that using RT, whereas it was 88–102 % using BL (1c) and 116–134 % using Equation (1d) of that using RT [see **Supporting Information—Table S3**]. Time resolution DS resulted in higher total light interception than HS, ca. 14 % higher using RT and 4 % higher using BL [see **Supporting Information—Table S3**].

Since additional information of lamina elevation angle was not required in Equations (1c) and (1d), and these two equations captured the middle-lower and the higher ranges, respectively, of I_i simulated by RT, we combined the two equations to create variability in I_i by a random factor ω (between 0 and 1 for individual leaves at a given time):

$$I_i = \min\,[\,I_i(1c),\ I_i(1d)\,]\ +\omega \times \{\max\,[\,I_i(1c)\,]$$
$$-\min\,[\,I_i(1c),\ I_i(1d)\,]\} - 0.3 \times (1-\omega) \times \min\,[\,I_i(1c),\ I_i(1d)\,]$$
$$(1e)$$

where I_i (1c) and I_i (1d) are the I_i simulated using Equation (1c) and Equation (1d), respectively. Using this equation, a variation of I_i around the minimum of I_i (1c) and I_i (1d) was generated, with a maximal value of I_i equal to the maximum of I_i (1c) and I_i (1d), and a minimal value of I_i equal to 70 % of the minimum of I_i (1c) and I_i (1d). The 30 % of variability for the lower I_i range chosen was consistent with the variability simulated by RT (1Q 18 %, median 31 %, mean 35 %, 3Q 45 %). Equation (1e) led to comparable estimation in leaf-level I_i/I_0 (Fig. 7A) and light interception (Fig. 7B; see **Supporting Information—Table S3**) to RT, and was used in the further BL simulations.

3.5 Comparison of predictive accuracies of dry matter production and photosynthetic acclimation using RT and using the BL

Dry matter production is the outcome of light acclimation and light-driven photosynthesis, reflecting integrative light–plant interaction from leaf to plant level. Shoot (total above-ground) dry matter was simulated under the conditions of experiments 1b, 2a and 2b using four combinations of model approaches and time-step resolutions, BL-DS, BL-HS, RT-DS and RT-HS, and compared to measured data (Fig. 8). The lowest accuracy (38.8 %, Fig. 8C) was achieved by RT-DS due to large overestimation, and the highest accuracy (83.0 %, Fig. 8B) by BL-HS, comparable to that of RT-HS (79.9 %, Fig. 8D). Both BL-HS and RT-HS were able to predict shoot dry matter under different treatments during different seasons with high accuracy, but the computational duration of RT-HS (64.4 ± 24.0 s per simulation day) was by one order of magnitude longer than the execution time of
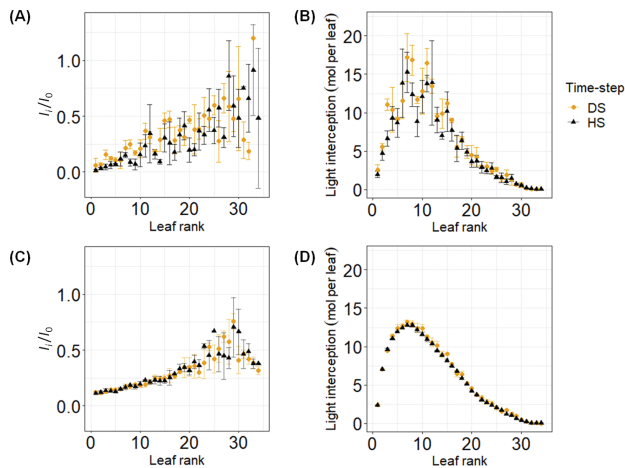
Figure 7. Comparison of simulated light conditions at leaf level using different light models and time resolutions. The models compared were (A, B) RT and (C, D) the BL (1e) in DS (DS, yellow circles) or HS (black triangles). (A, C) Snapshot of simulated relative PPFD (I_i/I_0) at 1200 h on the last day of 5-week of growth period, calculated as incident PPFD at each leaf divided by PPFD level above the canopy. (B, D) Total light interception (mol per leaf) summed over the 5-week growth period under the conditions of experiment 2a and treatment HLHN (for other treatments, see **Supporting Information—Table S3**).
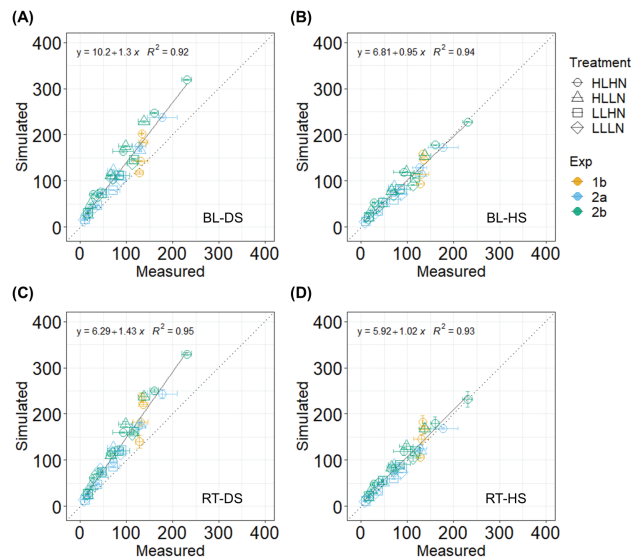

Figure 8. Model evaluation by comparing simulated shoot dry matter (g per plant) to measured data obtained in experiments 1b, 2a and 2b. Shoot dry matter including all above-ground dry matter of vegetative and reproductive parts was simulated (A) by BL (1e) in DS, (B) by BL in HS, (C) by RT and DS, (D) by RT and HS. Measured data were obtained in experiment 1b (yellow symbols), 2a (blue symbols) and 2b (green symbols) with three replications harvested between the second and the fifth weeks after transplanting into greenhouse (total 36 measured data points). Four combinations of light and nitrogen supply treatments (high light, HL, low light, LL, high nitrogen, HN, and low nitrogen, LN) applied in the experiments are indicated by different symbols. Dotted lines are one-to-one lines.

BL-HS (1.34 ± 0.16 s per simulation day). It should be noted that the computational duration to simulate k using RT was not accounted for in the case of BL-HS.

For both BL and RT approaches, time resolution of DS led to ca. 40 % (between 20 and 55 %) higher simulated shoot dry matter than HS [see **Supporting Information—Fig. S4A**], although DS only resulted in 14 % and 4 % higher total light interception per plant than HS using RT and BL, respectively [see **Supporting Information—Table S3**]. The overestimation by DS did not appear to result from a consistent overestimation of photosynthetic parameters, i.e. net photosynthesis rate measured at PPFD 1300 μmol m^{-2} s^{-1} (A_{n1300}; see **Supporting Information—Fig. S4B**), maximum electron transport rate (J_{max}; see **Supporting Information—Fig. S4C**) and maximum carboxylation rate (V_{cmax}; see **Supporting Information—Fig. S4D**). In the following comparisons of model performance, only simulations with HS were further examined.

Plant dry matter distribution was simulated with time resolution of HS and compared between RT and BL Equation (1e) (Table 3). Since dry matter distribution only depended on dry matter availability in a plant and not on light, it was directly affected by simulated shoot dry matter following a given priority scheme. Positive value of relative bias indicated a systematical overestimation of shoot and vegetative, while negative relative bias indicated underestimation of dry matter distribution to reproductive parts (Table 3). Following the same comparison, simulated leaf photosynthetic parameters were also examined with measured data obtained in experiment 2a. For all parameters examined, both BL and RT resulted in high accuracies between 71 and 82 %, except for maximum carboxylation rate (V_{cmax}) and respiration rate (R_d, Table

3), which were clearly over- and underestimated, respectively. In addition, both approaches tended to overestimate leaf chlorophyll (*Chl*) and photosynthetic nitrogen (N_p), and to underestimate net photosynthesis rate measured at PPFD 1300 μmol m^{-2} s^{-1} (A_{n1300}) and maximum electron transport rate (J_{max}). In summary, the performance of BL (1e) is comparable to and even slightly better than RT in predicting plant-level dry matter accumulation and leaf-level photosynthetic acclimation although there is still room for improvement in the functional part of the model, particularly dry matter distribution, V_{cmax} and R_d.

3.6 Sensitivity of predictive accuracy of dry matter production and photosynthetic acclimation to light extinction coefficient used

To test the sensitivity of model predictions to the k value used, constant values of k_c ranging 0.3–0.7 (in steps of 0.1) and a variable k_c calculated using Equation (2) were input into Equation (1c) to simulate plant dry matter in experiments 1b, 2a and 2b (Fig. 9A and C) and photosynthetic parameters in experiment 2a (Fig. 9B and D).

Among the constant k_c used, a k_c of 0.5 resulted in the highest accuracy (86.5 %) for shoot dry matter (Fig. 9A), and a deviation in k_c of 0.2 from k_c of 0.5 led to a decrease in accuracy by up to 27 %. When

Table 3. Predictive quality of light models using simple BL (1e) and using RT in HS. Plant dry matter variables simulated were vegetative and reproductive dry matter per plant and their sum as shoot dry matter. Photosynthetic acclimation variables simulated were net photosynthesis rate measured at PPFD 1300 μmol m^{-2} s^{-1} (A_{n1300}), maximum electron transport rate (J_{max}), maximum carboxylation rate (V_{cmax}), chlorophyll (Chl), photosynthetic nitrogen (N_p) and respiration rate (R_d). Measured data of plant dry matter were obtained in experiments 1b, 2a and 2b during the second and the fifth weeks after planting with three replications (total 36 measured data points). Leaf photosynthetic parameters were measured at two leaves per plant in experiment 2a for four consecutive weeks with two replications (total 32 measured data points).

| Light model	Accuracy (%)		Relative bias		RMSD (unit as variable)	
Variable			BL-HS	RT-HS		RT-HS
Shoot dry matter (g per plant)	83.0	79.9	0.037	0.164	14	16
Vegetative dry matter (g per plant)	62.8	56.5	0.540	0.742	20	24
Reproductive dry matter (g per plant)	43.9	46.3	−0.531	−0.474	15	14
A_{n1300} (μmol CO$_2$ m^{-2} s^{-1})	73.3	71.5	−0.342	−0.359	4.1	4.4
J_{max} (μmol e$^-$ m^{-2} s^{-1})	81.2	75.7	−0.127	−0.141	22	28
V_{cmax} (μmol CO$_2$ m^{-2} s^{-1})	72.2	67.6	0.250	0.227	17	20
Chl (mmol m^{-2})	80.3	79.7	0.305	0.263	0.085	0.087
N_p (mmol m^{-2})	82.2	78.4	0.151	0.121	6.9	8.3
R_d (μmol CO$_2$ m^{-2} s^{-1})	68.8	61.5	−0.384	−0.365	0.41	0.51
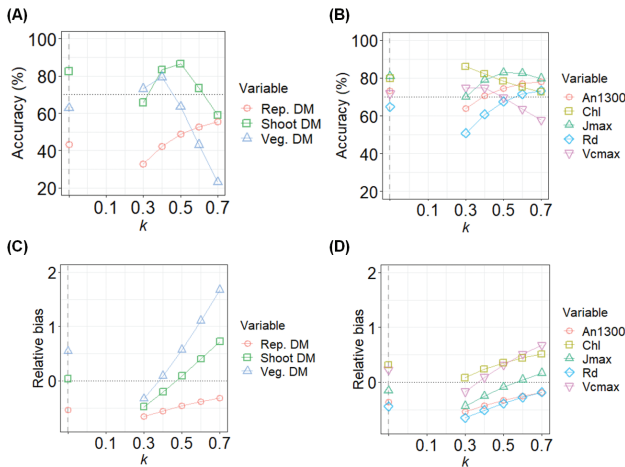
Figure 9. Effect of light extinction coefficient k_c on accuracy of predicting leaf photosynthetic acclimation and plant dry matter by BL (1c). Accuracies for (A) plant dry matter and (B) leaf photosynthetic parameters. Relative bias for (C) plant dry matter and (D) leaf photosynthetic parameters. Constant values of k_c between 0.3 and 0.7 were tested. Grey vertical dashed lines indicate the accuracy using variable k_c values estimated depending on canopy configuration by Equation (2).

distribution scheme towards vegetative parts. The accuracies of A_{n1300} and R_d increased with increasing k_c, and that of Chl and V_{cmax} increased with decreasing k (Fig. 9B), but the effects of k_c on these parameters were not as strong as on dry matter (Fig. 9A). Higher k_c values also resulted in higher simulated photosynthetic parameters (Fig. 9D), where a k_c of 0.5 resulted in the highest accuracy (82.9 %) for J_{max} (Fig. 9B).

In summary, BL (1c) with a constant k_c of 0.5 was able to predict plant dry matter production and leaf photosynthetic acclimation well (Fig. 9), justifying the applicability of a constant k using BL if an appropriate k could be first determined before model simulations were conducted. Although in this case the application of variable k values (Equation (2)) seemed somewhat redundant, it provided a proper k proxy without prior knowledge of k.

4.   DISCUSSION

In conjunction with a dynamic model of greenhouse cucumber, we compared the performance of 1D (BL) and 3D (RT) light modelling approaches in predicting leaf-level photosynthetic acclimation and plant-level dry matter accumulation over growth periods of 2–5 weeks. Prediction accuracy by BL Equation (1c) (Fig. 9) or Equation (1e) (Table 3) in combination with HS time resolution of simulation was found comparable to that by RT with HS (Table 3), when using light extinction coefficients k estimated following an empirical relationship (Equation (2)) established with the assistance of RT.

4.1 Applying the 3D light model enabled systematic examination of variation in light extinction coefficient k

The advantage of using the proposed relationship to estimate k as a function of L is that it provided a k proxy, whereby the effects of canopy geometry on k are taken into account. Motivated by similar intention,

using k_c values estimated by Equation (2) (indicated by the vertical grey line in Fig. 9A), the accuracy for shoot dry matter was 82.5 %, which was slightly lower than that by BL (1e) (83.0 %, Table 3). The higher the k_c used, the higher was the simulated plant dry matter and thus the higher the overestimation of shoot dry matter (Fig. 9C). The accuracy for vegetative dry matter peaked at a k_c of 0.4 (Fig. 9A), while that for reproductive dry matter increased with k_c, indicating a bias in

the effect of row spacing on k was examined experimentally in maize, sorghum, soybean and sun flower canopies by Flénet *et al.* (1996) as well as by a modelling approach in virtual gramineous canopies by Drouet and Kiniry (2008). Both found a decrease in k with increasing row spacing under the same plant density, consistent with our *in silico* measurements of k using RT (Fig. 4).

With information of canopy configuration, i.e. distance between rows (D_{row}) and distance between plants in a row (D_{plant}), minimal k (k_{min}) for a developed cucumber canopy was estimated using the empirical relationship Equation (2b) (Fig. 5A). In the given ranges of D_{row} between 1 and 2 m and D_{plant} between 0.1 and 1.0 m, k_{min} was found higher in more quadratic canopies, represented by a PR closer to one (Fig. 5B). With PR < 4, k_{min} tended to be higher under lower plant density, while over a PR of 4, k_{min} tended to be higher under higher plant density (Fig. 5B). The observation under lower PR can be intuitively understood in the sense of clumping at a scale of plant community. A quadratic distribution leads to lower clumping of plants in the field and thus higher k (Equation (1a)). Under high PR, individual plants are prone to aggregate within the row, but increasing plant density at the same PR reduces the gaps between the rows and slightly decreases clumping, thereby resulting in higher k (Fig. 5B). The experimental data obtained from maize canopies (Maddonni *et al.* 2001b) agreed with our *in silico* observation. At a density of 3 plants per m² and a leaf area index L ca. 2.5, a more square-distributed maize canopy with PR = 1.5 had higher k in comparison to that of a canopy with PR = 2.7. However, the effect of canopy geometry became insignificant under higher plants density (9 and 12 plants per m²), and k was found higher in the canopies with a plant density of 9 plants per m² (L of ca. 6) and 12 plants per m² (L of ca. 7) than the canopy with a density of 3 plants per m² (Maddonni *et al.* 2001b).

Although internode elongation and phototropism reacted to light signals in the current model, appearance of new phytomers, leaf expansion and petiole elongation exhibited no feedback response to these cues. Ignoring responses to light limitation and shading occurring at a high plant density, e.g. reduced leaf development and increased petiole elongation (Sessa *et al.* 2005; He *et al.* 2020), might lead to an underestimation of k due to unrealistically higher L and light transmission (I/I_0) using equation $k = -\ln(I/I_0)/L$. This increases the uncertainty of Equation (2b) under high plant density.

The values of k reported in literature for greenhouse cucumber vary from 0.42 to 0.87 [**see Supporting Information—Table S4**]. In addition to the effect of canopy geometry, seasonal solar position and diffuse light also contribute to this variation. Consistent with Equation (1a), a smaller solar zenith angle was found to result in lower k using a wheat FSPM (Evers *et al.* 2009), where in the most extreme case, a difference of 60° solar zenith led to a difference in k up to 0.48. The presence of diffuse light generally leads to lower k, although this effect interacts with solar angle (Li *et al.* 2014). These effects explain partly the lower k found in spring and summer (k between 0.4 and 0.6, from March to September) compared to autumn and winter (k > 0.8, from October to February; **see Supporting Information—Table S4**). The values of k in Fig. 4 was simulated from Julian day 206 to 227 under the conditions of experiment 1a (Table 1), where the solar zenith angle at 1200 h was 47° at the beginning and 35° at the end of the simulation. The effect of the zenith angle was intrinsically included in the k quantified by the 3D model. At the same location, the midday solar zenith can vary from 29° ($\cos\theta = 0.87$) at summer solstice to 76° ($\cos\theta = 0.24$) at winter solstice. Since in Equation (2b) these effects of incident light were not explicitly described (but see Eqs 5–8 in Lizaso *et al.* 2005), Equation (2) was only advisably applicable for conditions used in this study (as evaluated in Fig. 8B).

4.2 Simulation with different time resolutions revealed the impact of fluctuating light on dry matter accumulation

Higher dry matter accumulation in plants was predicted by simulations in DS (Fig. 8A and C) compared to HS (Fig. 8B and D), leading to an 20–55 % overestimation of dry matter with a trend of higher overestimation simulated by RT at Week 5 than that at Week 2 [**see Supporting Information—Fig. S4A**]. Since DS did not lead to apparent overestimation of photosynthetic parameters [**see Supporting Information—Fig. S4B–D**], this overestimation of plant dry matter could not be explained by the effect of photosynthetic acclimation. Although input total light integral per day was identical in both DS and HS, total plant light interception was ca. 14 % and 4 % higher in DS simulations at the end of a period of 5 weeks by RT and BL, respectively [**see Supporting Information—Table S3**], which still did not completely explain the extent of overestimation by DS. It can be argued that DS simulations approximate virtual plants photosynthesizing under constant light regime with an average daily light level without fluctuation during the day, whereas HS simulations approximate a growth light condition with natural fluctuation every hour. The phenomenon has been experimentally observed across C_3 and C_4 species. Compared to the plants grown under fluctuating light regimes, 19–140 % higher dry matter was accumulated under constant light regimes for the same daily light integral depending on plant species and the fluctuating pattern applied (Watling *et al.* 1997; Leakey *et al.* 2002; Kubásek *et al.* 2013; Vialet-Chabrand *et al.* 2017b; Sakoda *et al.* 2020). The discrepancy has been described as Jensen's inequality, a mathematical consequence of the non-linear functions where systematic bias aggregates from averaging values of the independent variable over a coarser scale than that experienced by the real system (Ruel and Ayres 1999). This applies especially to the asymptotic light response of photosynthesis since its response to changing light takes place rapidly at the scale of seconds to minutes, whereas the modification in photosynthetic proteins occurs at the scale of hours (Mettler *et al.* 2014). However, this effect has also been reported insignificant in tomato plants grown for 2–3 weeks (Kaiser *et al.* 2018; Y Zhang *et al.* 2020b), or reported to be opposite in an understory rainforest species *Micromelum minutum* (Watling *et al.* 1997). The large variability in the observations between species (Watling *et al.* 1997; Blom and Zheng 2009) may be explained by the species-specific biological effects (photosynthetic induction, e.g. Acevedo-Siaca *et al.* 2020; photoprotection, e.g. Niedermaier *et al.* 2020) in addition to the mathematical effect of Jensen's inequality. This pinpoints the avenues for further investigations of species-specific mechanisms of acclimation to dynamic light environments in both morphology and physiology (Vialet-Chabrand *et al.* 2017a; Pao *et al.* 2019b; Morales and Kaiser 2020; Y Zhang *et al.* 2020b).

4.3 Application of 1D light model facilitated predictions of average responses at whole-leaf and whole-plant levels

The choice of model depends on the scale of traits of interest (Jones *et al.* 2017). The general approach for constructing models is starting simple and then extending with details necessary for answering the question addressed, ensuring that the model is fit for purpose (Renton 2011; Auzmendi and Hanan 2020). The capability of FSPM to capture 3D distribution of environmental conditions and their interaction with plant architecture is necessary for a realistic representation and intuitive comprehension of the real systems (Vos *et al.* 2010) in order to answer research questions where spatial variability plays a crucial role, e.g. studying plant spacing, canopy structure manipulation and their interaction with lighting conditions from both solar and artificial sources (e.g. Buck-Sorlin *et al.* 2020). The advantage of FSPM enables mechanistic analyses of individual processes involved in architectural acclimation, assisting with identifying leaf- and canopy-level traits for improving cultural practices (e.g. Buck-Sorlin *et al.* 2011, 2020; Evers and Bastiaans 2016; N Zhang *et al.* 2020a) and selective breeding (e.g. Chen *et al.* 2014a; Perez *et al.* 2018). Here, we took advantage of the 3D light model to examine the effect of canopy geometry on light interception under various stages of canopy development (Fig. 4; **see Supporting Information—Fig. S3**), thereby establishing an estimation for k (Equation (2)) where the influences of diffuse light and solar zenith angle were integrated. The established estimation of k can then be applied to facilitate *in silico* experiments of various planting scenarios using 1D approach under the given environment. Since the current 3D model only takes the spatial distribution of light into account, physiological responses to other microclimate, e.g. temperature, relative humidity and CO_2 (but see Boulard *et al.* 2017; Ma *et al.* 2019), were not included. With future development of FSPMs, modelling biological response at a finer spatio-temporal scale would enable intelligible examinations in plant–environment interactions.

The application of 1D BL approach assumes homogeneity and isotropy of the canopies. This approximates well the conditions of evenly spaced, dense and closed canopies with randomly orientated and distributed canopy elements (Campbell and Norman 1989; Ponce de León and Bailey 2019), thereby well predicting the vertical extinction of direct solar radiation (Nilson 1971). For crops with fine and/or pinnate leaves with azimuthally symmetric orientation (e.g. wheat, tomato and palm), the assumptions appear to be adequate. However, for crops with large and compact leaves (e.g. cucumber and banana), high heterogeneity in the horizontal light distribution is expected, especially at the early developmental stages and in a row arrangement, where the assumptions are violated due to the large gaps in the plant community. Although presentation of light–plant interaction is restricted by using 1D model for cucumber canopies at an early developmental stage, its effect on carbon assimilation during this stage may not be significant to affect the total dry matter production at the scale of a later stage. Moreover, in a plant community with high ratio between its horizontal and vertical dimensions the horizontal heterogeneity may become recurrent, so that the probability of photon interception by individual plants still follows the Beer–Lambert law at the community level (Ponce de León and Bailey 2019; Bailey *et al.* 2020). The

impact of heterogeneity is expected to be further reduced under light condition consisting of diffuse light due to the high solar zenith angle (low elevation angle) of the incoming radiation (Ponce de León and Bailey 2019). Extensions and modifications have been proposed for the BL to partly include the variability in horizontal light distribution between canopies for row crops (Thornley and Johnson 1990), and by considering diffuse/direct light distribution in a canopy and shade/sunlit portion within a leaf (de Pury and Farquhar 1997; Lizaso *et al.* 2005; Roupsard *et al.* 2008; Govind 2014; Hikosaka 2014) depending on modelling aims.

Although canopy light interception and absorption can be well approximated using 1D light model, its suitability for predicting dry matter production is still unclear given the non-linearity of the light response of photosynthesis (Ponce de León and Bailey 2019). We showed that the classical models can be efficient tools for agronomic purposes. For simulating traits from whole-leaf (photosynthesis) to whole-plant (dry matter) level, the application of the simplest 1D light model following the BL (Equations (1c) and (1e)) reduced the computational demand without compromising the predictive accuracy of responses in the greenhouse cucumber canopies where high heterogeneity is expected. In summary, our results suggested that, with the assistance of the 3D plant structure and light model, the 1D light model using the BL provided efficient estimation for long-term processes integrating over weeks.

SUPPORTING INFORMATION
The following additional information is available in the online version of this article—

Note S1. Supplementary information of model description.

Table S1. Constants used to simulate phyllochron, leaf expansion and petiole elongation.

Table S2. Scenarios of plant densities and corresponding distances between rows and between plants simulated in Fig. 4.

Table S3. Simulated total light interception accumulated over a five-week growth period in experiment 2a.

Table S4. Reported light extinction coefficient k from literature for greenhouse cucumber crops.

Figure S1. Diagram of model data flow of the dynamic plant model of greenhouse cucumber.

Figure S2. Comparison of measured and simulated light interception efficiency at different leaves using ray tracing in hourly steps.

Figure S3. Simulated relationship between light extinction coefficient k and leaf area index of the canopy under different arrangements.

Figure S4. Overestimation by simulations in daily steps compared to in hourly steps of dry matter and photosynthetic parameters.

CONFLICT OF INTEREST

None declared.

CONTRIBUTIONS BY THE AUTHORS

Y.-C.P., T.-W.C., and H.S. conceived the study with input from K.K. Y.-C.P. constructed the model with contribution from T.-W.C. and D.W. Y.-C.P. performed the simulation and data analysis. Y.-C.P., K.K., and D.W. supervised and carried out the experimental data collection. Y.-C.P. took the lead in writing the manuscript. H.S., K.K., and T.-W.C. provided critical feedback and helped shape the analysis and interpretation. All authors discussed the results and contributed to the final manuscript.

LITERATURE CITED

Acevedo-Siaca LG, Coe R, Wang Y, Kromdijk J, Quick WP, Long SP. 2020. Variation in photosynthetic induction between rice accessions and its potential for improving productivity. *The New Phytologist* **227**:1097–1108.

Aubin I, Beaudet M, Messier C. 2000. Light extinction coefficients specific to the understory vegetation of the southern boreal forest, Quebec. *Canadian Journal of Forest Research* **30**:168–177.

Auzmendi I, Hanan JS. 2020. Investigating tree and fruit growth through functional-structural modelling: implications of carbon autonomy at different scales. *Annals of Botany* **126**:775–788.

Bailey BN, Ponce de León MA, Krayenhoff ES. 2020. One-dimensional models of radiation transfer in heterogeneous canopies: a review, re-evaluation, and improved model. *Geoscientific Model Development* **13**:4789–4808.

Blom TJ, Zheng Y. 2009. The response of plant growth and leaf gas exchange to the speed of lamp movement in a greenhouse. *Scientia Horticulturae* **119**:188–192.

Boulard T, Roy J-C, Pouillard J-B, Fatnassi H, Grisey A. 2017. Modelling of micrometeorology, canopy transpiration and photosynthesis in a closed greenhouse using computational fluid dynamics. *Biosystems Engineering* **158**:110–133.

Buckley TN, Cescatti A, Farquhar GD. 2013. What does optimization theory actually predict about crown profiles of photosynthetic capacity when models incorporate greater realism? *Plant, Cell & Environment* **36**:1547–1563.

Buck-Sorlin GH, Cornilleau X, Rahme S, Truffault V, Brajeul E. 2020. A functional-structural plant model of greenhouse-grown cucumber under LED lighting. *Acta Horticulturae* **1296**:381–388.

Buck-Sorlin GH, de Visser PH, Henke M, Sarlikioti V, van der Heijden GW, Marcelis LF, Vos J. 2011. Towards a functional-structural plant model of cut-rose: simulation of light environment, light absorption, photosynthesis and interference with the plant structure. *Annals of Botany* **108**:1121–1134.

Buck-Sorlin GH, Hemmerling R, Vos J, de Visser PHB. 2010. Modelling of spatial light distribution in the greenhouse: description of the model. In: Li B, Jaeger M, Guo Y, eds. *Proceedings of the Third International Symposium on Plant Growth Modeling, Simulation, Visualization and Applications - PMA09*. 9–13 November 2009. Beijing, China: IEEE Computer Society Conference Publishing Services, 79–86.

Cabrera-Bosquet L, Fournier C, Brichet N, Welcker C, Suard B, Tardieu F. 2016. High-throughput estimation of incident light, light interception and radiation-use efficiency of thousands of plants in a phenotyping platform. *The New Phytologist* **212**:269–281.

Campbell GS, Norman JM. 1989. The description and measurement of plant canopy structure. In: Russell G, Marshall B, Jarvis PG, eds. *Plant canopies: their growth, form and function*, vol. **31**. Cambridge: Cambridge University Press, 1–19.

Charles-Edwards DA, Doley D, Rimmington GM. 1986. *Modelling plant growth and development*. Sydney: Academic Press.

Chelle M, Andrieu B. 1999. Radiative models for architectural modeling. *Agronomie* **19**:225–240.

Chen JM, Black TA. 1991. Measuring leaf area index of plant canopies with branch architecture. *Agricultural and Forest Meteorology* **57**:1–12.

Chen TW, Cabrera-Bosquet L, Alvarez Prado S, Perez R, Artzet S, Pradal C, Coupel-Ledru A, Fournier C, Tardieu F. 2019. Genetic and environmental dissection of biomass accumulation in multi-genotype maize canopies. *Journal of Experimental Botany* **70**:2523–2534.

Chen TW, Henke M, de Visser PH, Buck-Sorlin G, Wiechers D, Kahlen K, Stützel H. 2014a. What is the most prominent factor limiting photosynthesis in different layers of a greenhouse cucumber canopy? *Annals of Botany* **114**:677–688.

Chen TW, Nguyen TM, Kahlen K, Stützel H. 2014b. Quantification of the effects of architectural traits on dry mass production and light interception of tomato canopy under different temperature regimes using a dynamic functional-structural plant model. *Journal of Experimental Botany* **65**:6399–6410.

De Costa WAJM de, Dennett MD. 1992. Is canopy light extinction coefficient a species-specific constant? *Tropical Agricultural Research* **4**:123–137.

de Pury DGG, Farquhar GD. 1997. Simple scaling of photosynthesis from leaves to canopies without the errors of big-leaf models. *Plant, Cell & Environment* **20**:537–557.

Drouet J-L, Kiniry JR. 2008. Does spatial arrangement of 3D plants affect light transmission and extinction coefficient within maize crops? *Field Crops Research* **107**:62–69.

Duursma RA, Falster DS, Valladares F, Sterck FJ, Pearcy RW, Lusk CH, Sendall KM, Nordenstahl M, Houter NC, Atwell BJ, Kelly N, Kelly JW, Liberloo M, Tissue DT, Medlyn BE, Ellsworth DS. 2012. Light interception efficiency explained by two simple variables: a test using a diversity of small- to medium-sized woody plants. *The New Phytologist* **193**:397–408.

Evans JR. 1993. Photosynthetic acclimation and nitrogen partitioning within a lucerne canopy. II. Stability through time and comparison with a theoretical optimum. *Functional Plant Biology* **20**:69–82.

Evers JB, Bastiaans L. 2016. Quantifying the effect of crop spatial arrangement on weed suppression using functional-structural plant modelling. *Journal of Plant Research* **129**:339–351.

Evers JB, Huth NI, Renton M. 2009. Light extinction in spring wheat canopies in relation to crop configuration and solar angle. In: *2009 Third International Symposium on Plant Growth Modeling, Simulation, Visualization and Applications (PMA)*. Beijing: IEEE, 107–110.

Farquhar GD, von Caemmerer S, Berry JA. 1980. A biochemical model of photosynthetic CO_2 assimilation in leaves of C_3 species. *Planta* **149**:78–90.

Flénet F, Kiniry JR, Board JE, Westgate ME, Reicosky DC. 1996. Row spacing effects on light extinction coefficients of corn, sorghum, soybean, and sunflower. *Agronomy Journal* **88**:185–190.

Forrester DI. 2014. A stand-level light interception model for horizontally and vertically heterogeneous canopies. *Ecological Modelling* **276**:14–22.

Forsythe WC, Rykiel EJ Jr, Stahl RS, Wu H-i, Schoolfield RM. 1995. A model comparison for daylength as a function of latitude and day of year. *Ecological Modelling* **80**:87–95.

Govind A. 2014. On the nature of canopy illumination due to differences in elemental orientation and aggregation for radiative transfer. *International Journal of Biometeorology* **58**:1803–1809.

He L, Sun W, Chen X, Han L, Li J, Ma Y, Song Y. 2020. Modeling maize canopy morphology in response to increased plant density. *Frontiers in Plant Science* **11**:533514.

Hikosaka K. 2014. Optimal nitrogen distribution within a leaf canopy under direct and diffuse light. *Plant, Cell & Environment* **37**:2077–2085.

Hofmann M, Seckmeyer G. 2017. A new model for estimating the diffuse fraction of solar irradiance for photovoltaic system simulations. *Energies* **10**:248.

Irving LJ, Robinson D. 2006. A dynamic model of Rubisco turnover in cereal leaves. *The New Phytologist* **169**:493–504.

Jones JW, Antle JM, Basso B, Boote KJ, Conant RT, Foster I, Godfray HCJ, Herrero M, Howitt RE, Janssen S, Keating BA, Munoz-Carpena R, Porter CH, Rosenzweig C, Wheeler TR. 2017. Brief history of agricultural systems modeling. *Agricultural Systems* **155**:240–254.

Kahlen K. 2006. 3D architectural modelling of greenhouse cucumber (*Cucumis sativus* L.) using L-systems. *Acta Horticulturae* **718**:51–58.

Kahlen K, Chen TW. 2015. Predicting plant performance under simultaneously changing environmental conditions—the interplay between temperature, light, and internode growth. *Frontiers in Plant Science* **6**:1130.

Kahlen K, Stützel H. 2007. Estimation of geometric attributes and masses of individual cucumber organs using three-dimensional digitizing and allometric relationships. *Journal of the American Society for Horticultural Science* **132**:439–446.

Kahlen K, Stützel H. 2011. Modelling photo-modulated internode elongation in growing glasshouse cucumber canopies. *The New Phytologist* **190**:697–708.

Kahlen K, Wiechers D, Stützel H. 2008. Modelling leaf phototropism in a cucumber canopy. *Functional Plant Biology* **35**:876–884.

Kaiser E, Matsubara S, Harbinson J, Heuvelink E, Marcelis LFM. 2018. Acclimation of photosynthesis to lightflecks in tomato leaves: interaction with progressive shading in a growing canopy. *Physiologia Plantarum* **162**:506–517.

Kang M, Heuvelink E, Carvalho SMP, de Reffye P. 2012. A virtual plant that responds to the environment like a real one: the case for chrysanthemum. *The New Phytologist* **195**:384–395.

Kniemeyer O. 2008. *Design and implementation of a graph grammar based language for functional-structural plant modelling.* Doctoral Dissertation, Brandenburg University of Technology, Cottbus-Senftenberg, Germany.

Kubásek J, Urban O, Šantrůček J. 2013. C_4 plants use fluctuating light less efficiently than do C_3 plants: a study of growth, photosynthesis and carbon isotope discrimination. *Physiologia Plantarum* **149**:528–539.

Kuwar G. 2007. *Modelling dry matter partitioning in greenhouse cucumber: modelling dry matter partitioning in greenhouse.* MSc, Leibniz Universität Hannover, Germany.

Leakey ADB, Press MC, Scholes JD, Watling JR. 2002. Relative enhancement of photosynthesis and growth at elevated CO_2 is greater under sunflecks than uniform irradiance in a tropical rain forest tree seedling. *Plant, Cell & Environment* **25**:1701–1714.

Li T, Heuvelink E, Dueck TA, Janse J, Gort G, Marcelis LF. 2014. Enhancement of crop photosynthesis by diffuse light: quantifying the contributing factors. *Annals of Botany* **114**:145–156.

Lizaso JI, Batchelor WD, Boote KJ, Westgate ME. 2005. Development of a leaf-level canopy assimilation model for CERES-Maize. *Agronomy Journal* **97**:722–733.

Louarn G, Song Y. 2020. Two decades of functional-structural plant modelling: now addressing fundamental questions in systems biology and predictive ecology. *Annals of Botany* **126**:501–509.

Ludlow MM. 1983. External factors influencing photosynthesis and respiration. In: Dale JE, Milthorpe FL, eds. *The growth and functioning of leaves*. Cambridge: Cambridge University Press, 347–380.

Ma D, Carpenter N, Maki H, Rehman TU, Tuinstra MR, Jin J. 2019. Greenhouse environment modeling and simulation for microclimate control. *Computers and Electronics in Agriculture* **162**:134–142.

Maddonni GA, Chelle M, Drouet J-L, Andrieu B. 2001a. Light interception of contrasting azimuth canopies under square and rectangular plant spatial distributions: simulations and crop measurements. *Field Crops Research* **70**:1–13.

Maddonni GA, Otegui ME, Cirilo AG. 2001b. Plant population density, row spacing and hybrid effects on maize canopy architecture and light attenuation. *Field Crops Research* **71**:183–193.

Marcelis LF. 1994. A simulation model for dry matter partitioning in cucumber. *Annals of Botany* **74**:43–52.

Mettler T, Mühlhaus T, Hemme D, Schöttler MA, Rupprecht J, Idoine A, Veyel D, Pal SK, Yaneva-Roder L, Winck FV, Sommer F, Vosloh D, Seiwert B, Erban A, Burgos A, Arvidsson S, Schönfelder S, Arnold A, Günther M, Krause U, Lohse M, Kopka J, Nikoloski Z, Mueller-Roeber B, Willmitzer L, Bock R, Schroda M, Stitt M. 2014. Systems analysis of the response of photosynthesis, metabolism, and growth to an increase in irradiance in the photosynthetic model organism *Chlamydomonas reinhardtii*. *The Plant Cell* **26**:2310–2350.

Monsi M, Saeki T. 2005. On the factor light in plant communities and its importance for matter production. 1953. *Annals of Botany* **95**:549–567.

Morales A, Kaiser E. 2020. Photosynthetic acclimation to fluctuating irradiance in plants. *Frontiers in Plant Science* **11**:268.

Moualeu-Ngangue DP, Chen TW, Stützel H. 2016. A modeling approach to quantify the effects of stomatal behavior and mesophyll conductance on leaf water use efficiency. *Frontiers in Plant Science* **7**:875.

Niedermaier S, Schneider T, Bahl MO, Matsubara S, Huesgen PF. 2020. Photoprotective acclimation of the *Arabidopsis thaliana* leaf proteome to fluctuating light. *Frontiers in Genetics* **11**:154.

Nilson T. 1971. A theoretical analysis of the frequency of gaps in plant stands. *Agricultural Meteorology* **8**:25–38.

Pao YC, Chen TW, Moualeu-Ngangue DP, Stützel H. 2019a. Environmental triggers for photosynthetic protein turnover

determine the optimal nitrogen distribution and partitioning in the canopy. *Journal of Experimental Botany* **70**:2419–2434.

Pao YC, Chen TW, Moualeu-Ngangue DP, Stützel H. 2020. Experiments for *in silico* evaluation of optimality of photosynthetic nitrogen distribution and partitioning in the canopy: an example using greenhouse cucumber plants. *Bio-Protocol* **10**:e3556.

Pao YC, Stützel H, Chen TW. 2019b. A mechanistic view of the reduction in photosynthetic protein abundance under diurnal light fluctuation. *Journal of Experimental Botany* **70**:3705–3708.

Perez RPA, Dauzat J, Pallas B, Lamour J, Verley P, Caliman JP, Costes E, Faivre R. 2018. Designing oil palm architectural ideotypes for optimal light interception and carbon assimilation through a sensitivity analysis of leaf traits. *Annals of Botany* **121**:909–926.

Ponce de León MA, Bailey BN. 2019. Evaluating the use of Beer's law for estimating light interception in canopy architectures with varying heterogeneity and anisotropy. *Ecological Modelling* **406**:133–143.

Qian T, Elings A, Dieleman JA, Gort G, Marcelis LFM. 2012. Estimation of photosynthesis parameters for a modified Farquhar–von Caemmerer–Berry model using simultaneous estimation method and nonlinear mixed effects model. *Environmental and Experimental Botany* **82**:66–73.

Reindl DT, Beckman WA, Duffie JA. 1990. Diffuse fraction correlations. *Solar Energy* **45**:1–7.

Renton M. 2011. How much detail and accuracy is required in plant growth sub-models to address questions about optimal management strategies in agricultural systems? *AoB Plants* **2011**:plr006; doi:10.1093/aobpla/plr006.

Roupsard O, Dauzat J, Nouvellon Yann, Deveau A, Feintrenie L, Saint-André L, Mialet-Serra I, Braconnier S, Bonnefond J-M, Berbigier P, Epron D, Jourdan C, Navarro M, Bouillet J-P. 2008. Cross-validating sun-shade and 3D models of light absorption by a tree-crop canopy. *Agricultural and Forest Meteorology* **148**:549–564.

Ruel JJ, Ayres MP. 1999. Jensen's inequality predicts effects of environmental variation. *Trends in Ecology & Evolution* **14**:361–366.

Sakoda K, Yamori W, Shimada T, Sugano SS, Hara-Nishimura I, Tanaka Y. 2020. Higher stomatal density improves photosynthetic induction and biomass production in *Arabidopsis* under fluctuating light. *Frontiers in Plant Science* **11**:589603.

Sarlikioti V, de Visser PH, Buck-Sorlin GH, Marcelis LF. 2011a. How plant architecture affects light absorption and photosynthesis in tomato: towards an ideotype for plant architecture using a functional-structural plant model. *Annals of Botany* **108**:1065–1073.

Sarlikioti V, de Visser PH, Marcelis LF. 2011b. Exploring the spatial distribution of light interception and photosynthesis of canopies by means of a functional-structural plant model. *Annals of Botany* **107**:875–883.

Schmidt D, Kahlen K. 2019. Positional variation rather than salt stress dominates changes in three-dimensional leaf shape patterns in cucumber canopies. *In Silico Plants* **1**:diz011; doi:10.1093/insilicoplants/diz011.

Tahiri AZ, Anyoji H, Yasuda H. 2006. Fixed and variable light extinction coefficients for estimating plant transpiration and soil evaporation under irrigated maize. *Agricultural Water Management* **84**:186–192.

Thornley JHM, Johnson IR. 1990. *Plant and crop modelling*. Oxford: Clarendon Press.

van Henten EJ, Hemming J, van Tuijl BAJ, Kornet JG, Meuleman J, Bontsema, J, van Os EA. 2002. An autonomous robot for harvesting cucumbers in greenhouses. *Autonomous Robots* **13**:241–258.

Vialet-Chabrand SRM, Matthews JSA, McAusland L, Blatt MR, Griffiths H, Lawson T. 2017a. Temporal dynamics of stomatal behavior: modeling and implications for photosynthesis and water use. *Plant Physiology* **174**:603–613.

Vialet-Chabrand SRM, Matthews JS, Simkin AJ, Raines CA, Lawson T. 2017b. Importance of fluctuations in light on plant photosynthetic acclimation. *Plant Physiology* **173**:2163–2179.

von Elsner B, Briassoulis D, Waaijenberg D, Mistriotis A, von Zabeltitz C, Gratraud J, Russo G, Suay-Cortes R. 2000. Review of structural and functional characteristics of greenhouses in European Union countries: part I, design requirements. *Journal of Agricultural Engineering Research* **75**:1–16.

Vos J, Evers JB, Buck-Sorlin GH, Andrieu B, Chelle M, de Visser PH. 2010. Functional-structural plant modelling: a new versatile tool in crop science. *Journal of Experimental Botany* **61**:2101–2115.

Warren Wilson J, Hand DW, Hannah MA. 1992. Light interception and photosynthetic efficiency in some glasshouse crops. *Journal of Experimental Botany* **43**:363–373.

Watling JR, Ball MC, Woodrow IE. 1997. The utilization of lightflecks for growth in four Australian rain-forest species. *Functional Ecology* **11**:231–239.

Wiechers D, Kahlen K, Stützel H. 2011a. Dry matter partitioning models for the simulation of individual fruit growth in greenhouse cucumber canopies. *Annals of Botany* **108**:1075–1084.

Wiechers D, Kahlen K, Stützel H. 2011b. Evaluation of a radiosity based light model for greenhouse cucumber canopies. *Agricultural and Forest Meteorology* **151**:906–915.

Zhang B, DeAngelis DL. 2020. An overview of agent-based models in plant biology and ecology. *Annals of Botany* **126**:539–557.

Zhang L, Hu Z, Fan J, Zhou D, Tang F. 2014. A meta-analysis of the canopy light extinction coefficient in terrestrial ecosystems. *Frontiers of Earth Science* **8**:599–609.

Zhang N, van Westreenen A, Evers JB, Anten NPR, Marcelis LFM. 2020a. Quantifying the contribution of bent shoots to plant photosynthesis and biomass production of flower shoots in rose (*Rosa hybrida*) using a functional-structural plant model. *Annals of Botany* **126**:587–599.

Zhang Y, Kaiser E, Marcelis LFM, Yang Q, Li T. 2020b. Salt stress and fluctuating light have separate effects on photosynthetic acclimation, but interactively affect biomass. *Plant, Cell & Environment* **43**:2192–2206.